Int. J Solids Structures Vol. 23, No 2, pp. 287–303, 1987
Printed in Great Britain.

0020–7683/87 $3.00+.00

ON THE LATERAL HARMONIC MOTION OF AN ELASTIC BAR EMBEDDED IN AN ELASTIC HALF-SPACE

R. K. N. D. RAJAPAKSE and A. H. SHAH
Department of Civil Engineering, University of Manitoba, Winnipeg, Canada R3T 2N2

(*Received* 25 *November* 1985; *in revised form* 2 *May* 1986)

Abstract—This study is concerned with the dynamic response of a long cylindrical elastic bar which is partially embedded in a homogeneous elastic half-space and is subjected to a harmonic lateral load, or to a moment. Appropriate asymmetric Green's functions are derived through Hankel integral transforms and are presented explicitly. An efficient solution scheme based on Lagrange's equation of motion combined with a discretization technique is applied to solve the title problem. Numerical results are presented to illustrate the influence of bar flexibility, mass density, geometry, and frequency of excitation on the horizontal, moment (rocking), and coupled impedances of the bar–elastic half-space system.

INTRODUCTION

The study of finite cylindrical elastic bars which are partially embedded in an elastic half-space and subjected to a harmonic lateral load or to a moment as shown in Fig. 1 has useful application in several branches of engineering. The force–displacement relationship (impedance) of such a system in particular has direct application in the analysis of pile foundations under dynamic loading. A review of existing literature reveals that an exact analytical formulation is not available even for the case of a laterally loaded rigid bar under static loading. Among the existing solutions, the most rigorous treatment on the static problem is due to Apirathvorakij and Karasudhi[1]. They extended the solution scheme developed by Muki and Sternberg[2] for elastostatic axial load transfer to study the quasi-static bending of a long cylindrical elastic bar partially embedded in a saturated porous elastic half-space. A recent study by Karasudhi *et al.*[3] investigated the effect of a modified compatibility condition.

A less rigorous approach was presented by Spillers and Stoll[4] to study the behaviour of laterally loaded elastic piles under static loading. In Ref. [4], the pile was modelled as a line inclusion which obeys the Bernoulli–Euler beam theory and the interactive reaction

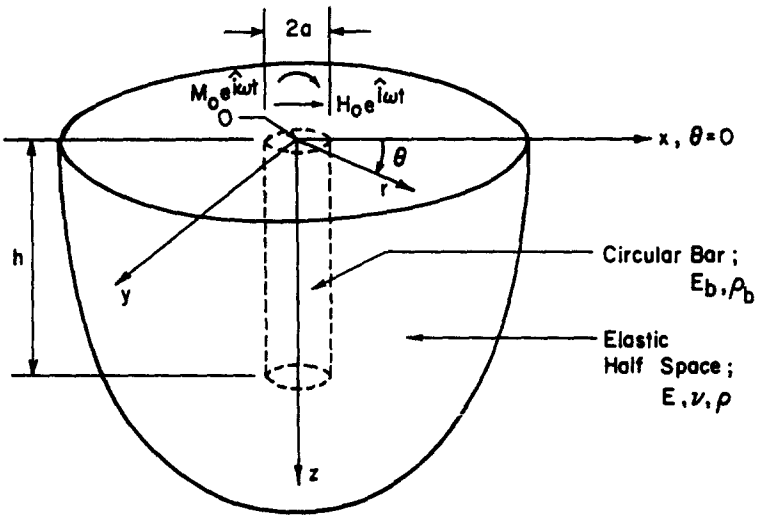

Fig. 1. Geometry of bar and embedding medium.

between the beam and the half-space was modelled by a horizontal point load acting in the interior of a half-space[5]. The study of Ref. [4] provided the basis for the currently utilized discretization technique. Improvements to the work of Ref. [4] have been reported by Poulos[6], Butterfield and Bannerjee[7], and Selvadurai and Rajapakse[8].

Studies on the dynamic problem are rather limited. Nogami and Novak[9, 10] presented a solution for an elastic pile embedded in a soil layer of equal height resting on a rigid base. This analysis was based on a two-dimensional representation where both the displacement and the equilibrium equations of the soil layer in a vertical direction was neglected to obtain a simpler solution. In a recent study, Nielsen[11] investigated the resistance of an elastic layer to a given horizontal displacement profile, and found that the use of true three-dimensional conditions for the soil layer yields results which are greatly different from those in Ref. [9]. The most rigorous treatment on the problem of a dynamically loaded rigid cylinder embedded in an elastic half-space is due to Apsel[12], who presented a solution based on the boundary integral equation technique. Recently, Sen *et al.*[13] made an attempt to solve the problem of a finite elastic bar embedded in an elastic half-space and subjected to a lateral dynamic load, by extending the scheme of Ref. [4].

In a previous paper[14], the authors discussed in detail the deficiencies associated with the application of the solution scheme employed in Ref. [13] to solve the elastodynamic problem. Thus, an accurate solution accounting for the three-dimensional behaviour of the surrounding medium is currently not available for the title problem. In this study, the authors have extended their solution scheme developed for the longitudinal vibration[14] to determine the impedance of the system shown in Fig. 1.

Initially Green's functions corresponding to appropriate asymmetric ring loads acting in the interior of the half-space are derived by employing Hankel integral transforms, and are presented explicitly. These Green's functions are used to develop the influence functions required in the proposed solution scheme. The solution scheme presented in this study is based on the assumption that the length to radius ratio of the bar is large, and the frequency of excitation is small, such that the use of the Bernoulli–Euler beam theory for the bar is justifiable. In view of these assumptions, the lateral displacement of the bar is approximated by an admissible function of the z-coordinate containing a set of generalized coordinates. These generalized coordinates are determined through the application of Lagrange's equation of motion to the bar–half-space system.

Numerical results are presented to verify the accuracy and convergence of the present solution scheme. The influence of bar geometry (length/radius ratio), bar flexibility ratio, mass density and frequency of excitation on the lateral, rocking, and coupled impedances of the bar–half-space system shown in Fig. 1 is illustrated by means of a parametric study.

FUNDAMENTAL SOLUTIONS

Consider a half-space region as shown in Fig. 2, in which (r, θ, z) is the cylindrical polar coordinate system, and the related rectangular Cartesian coordinate system (x, y, z) is such that the z-axis is normal to the free surface. For an isotropic linear elastic medium, the displacements u, v, and w in the r-, θ-, and z-directions, respectively, can be expressed in terms of three scalar potential functions as

$$u = \frac{\partial \phi}{\partial r} + \frac{\partial^2 \psi}{\partial r \partial z} + \frac{1}{r}\frac{\partial \Lambda}{\partial \theta} \tag{1a}$$

$$v = \frac{1}{r}\frac{\partial \phi}{\partial \theta} + \frac{1}{r}\frac{\partial^2 \psi}{\partial \theta \partial z} - \frac{\partial \Lambda}{\partial r} \tag{1b}$$

$$w = \frac{\partial \phi}{\partial z} - \left[\frac{1}{r}\frac{\partial}{\partial r}\left(r\frac{\partial}{\partial r}\right) + \frac{1}{r^2}\frac{\partial^2}{\partial \theta^2}\right]\psi. \tag{1c}$$

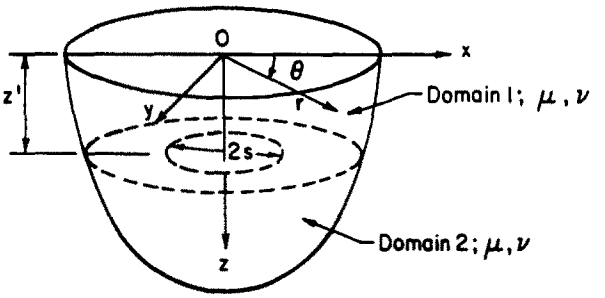

Fig. 2. System considered in deriving the fundamental solution.

In view of the representation given by eqns (1a)–(1c), together with consideration of harmonic vibrations of circular frequency ω characterized by the term $e^{i\omega t}$ (suppressed in the sequel) where $i = \sqrt{-1}$, the displacement equations of equilibrium in the absence of body forces are satisfied if the potentials ϕ, ψ and Λ are the solutions to the following scalar wave equations:

$$(\nabla^2 + k_p^2)\phi = 0 \tag{2a}$$

$$(\nabla^2 + k_s^2)\psi = 0 \tag{2b}$$

$$(\nabla^2 + k_s^2)\Lambda = 0 \tag{2c}$$

where $k_p^2 = \omega^2\rho/(\lambda + 2\mu)$ and $k_s^2 = \omega^2\rho/\mu$ are the pressure and shear wave numbers, respectively; λ and μ are Lame's constants; ρ the density of the medium, and ∇^2 is the Laplacian operator. The representations of eqns (1a)–(1c) can be expanded by Fourier expansions with respect to the θ-coordinate. In doing so, the potentials of ϕ, ψ and Λ can be expressed as

$$\phi(r,\theta,z) = \sum_{m=0}^{\infty} \phi_m(r,z)\begin{Bmatrix}\cos m\theta \\ \sin m\theta\end{Bmatrix} \tag{3a}$$

$$\psi(r,\theta,z) = \sum_{m=0}^{\infty} \psi_m(r,z)\begin{Bmatrix}\cos m\theta \\ \sin m\theta\end{Bmatrix} \tag{3b}$$

$$\Lambda(r,\theta,z) = \sum_{m=0}^{\infty} \Lambda_m(r,z)\begin{Bmatrix}\sin m\theta \\ -\cos m\theta\end{Bmatrix}. \tag{3c}$$

Substitution of the representation given by eqns (3a)–(3c) in eqns (2a)–(2c) together with the use of Hankel integral transforms[15] leads to the following solution for Fourier components ϕ_m, ψ_m, and Λ_m

$$\phi_m(r,z) = \int_0^{\infty} \xi(A_m e^{-\alpha z} + B_m e^{\alpha z})J_m(\xi r)\,d\xi \tag{4a}$$

$$\psi_m(r,z) = \int_0^{\infty} \xi(C_m e^{-\beta z} + D_m e^{\beta z})J_m(\xi r)\,d\xi \tag{4b}$$

$$\Lambda_m(r,z) = \int_0^{\infty} \xi(E_m e^{-\beta z} + F_m e^{\beta z})J_m(\xi r)\,d\xi \tag{4c}$$

$$\alpha = (\xi^2 - k_p^2)^{1/2}, \qquad \xi > k_p$$
$$= \hat{\imath}(k_p^2 - \xi^2)^{1/2}, \qquad \xi < k_p \tag{5a}$$

$$\beta = (\xi^2 - k_s^2)^{1/2}, \qquad \xi > k_s$$
$$= \hat{\imath}(k_s^2 - \xi^2)^{1/2}, \qquad \xi < k_s. \tag{5b}$$

In eqns (4a)–(4c), ξ is the Hankel transform parameter, J_m is the Bessel function of the first kind of order m, and $A_m(\xi)$, $B_m(\xi)$, $C_m(\xi)$, $D_m(\xi)$, $E_m(\xi)$, and $F_m(\xi)$ are arbitrary functions to be determined by invoking appropriate boundary and continuity conditions. In view of eqns (1), (3), and (4), the displacements $u(r,\theta,z)$, $v(r,\theta,z)$, and $w(r,\theta,z)$ can be expanded in terms of Fourier components $u_m(r,z)$, $v_m(r,z)$, and $w_m(r,z)$, respectively. These Fourier components are found to be

$$w_m(r,z) = \int_0^\infty [\alpha(-A_m e^{-\alpha z} + B_m e^{\alpha z}) + \xi^2(C_m e^{-\beta z} + D_m e^{\beta z})]\xi J_m(\xi r)\,d\xi \tag{6a}$$

$$u_m \pm v_m = \int_0^\infty [\mp(A_m e^{-\alpha z} + B_m e^{\alpha z}) \mp \beta(-C_m e^{-\beta z} + D_m e^{\beta z}) + (E_m e^{-\beta z} + F_m e^{\beta z})]\xi^2 J_{m\pm1}(\xi r)\,d\xi. \tag{6b}$$

The relevant stress components $\sigma_{zz}(r,\theta,z)$, $\sigma_{zr}(r,\theta,z)$, and $\sigma_{z\theta}(r,\theta,z)$ in the present class of problems can be expanded in an identical manner in terms of Fourier components $\sigma_{zz}^m(r,z)$, $\sigma_{zr}^m(r,z)$ and $\sigma_{z\theta}^m(r,z)$, respectively. With appropriate manipulations, σ_{zz}^m, σ_{zr}^m and $\sigma_{z\theta}^m$ can be expressed as

$$\sigma_{zz}^m(r,z) = \mu \int_0^\infty [(2\xi^2 - k_s^2)(A_m e^{-\alpha z} + B_m e^{\alpha z}) + 2\beta\xi^2(-C_m e^{-\beta z} + D_m e^{\beta z})]\xi J_m(\xi r)\,d\xi \tag{7a}$$

$$\sigma_{zr}^m \pm \sigma_{z\theta}^m = \mu \int_0^\infty [\mp 2\alpha(-A_m e^{-\alpha z} + B_m e^{\alpha z}) \mp (2\xi^2 - k_s^2)(C_m e^{-\beta z} + D_m e^{\beta z}) + \beta(-E_m e^{-\beta z} + F_m e^{\beta z})]\xi^2 J_{m\pm1}\,d\xi. \tag{7b}$$

The displacements and stresses given by eqns (6) and (7) could be used to represent the general solution to problems having axisymmetric geometry subjected to arbitrary loading. Note that the system shown in Fig. 1 possesses symmetry about the x-axis ($\theta = 0$), and the relevant displacements and stresses are obtained from eqns (6) and (7) by considering only a single symmetric term in the Fourier expansion with $m = 1$.

At this stage, it is convenient to nondimensionalize the problem under consideration by defining a length parameter "a", which denotes the radius of the embedded cylindrical bar; a is taken as a unit of length. Consider the problem of a homogeneous half-space subjected to concentrated circular ring loads in the x- and z-directions as shown in Figs 3(a) and (b). Solutions corresponding to these loading configurations can be obtained by considering two domain problems as suggested in Ref. [8] for the corresponding static problem. The boundary and continuity conditions remain identical to the static problem as given in Ref. [8]. The solution of the associated boundary value problems results in the expressions for displacement corresponding to each loading case, and these expressions are given by eqns (A1)–(A6) in the appendix.

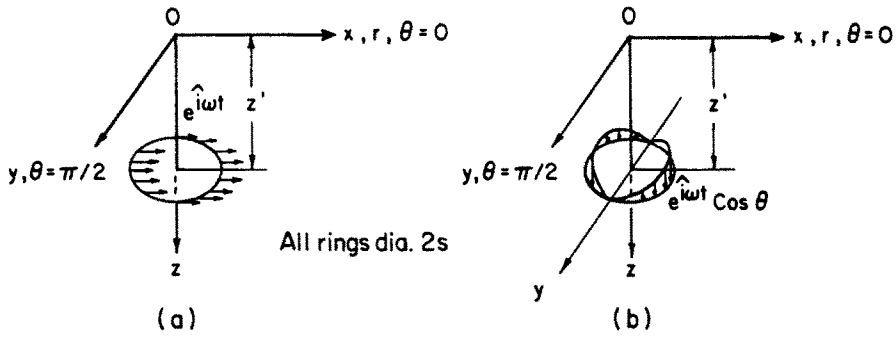

Fig. 3. Concentrated ring loads acting in the interior of the half-space.

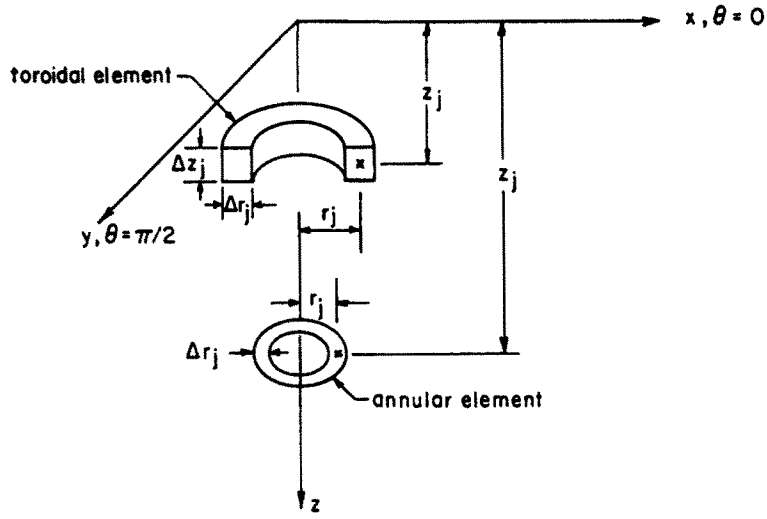

Fig. 4. Geometry of the toroidal and annular elements.

In the subsequent section dealing with the system shown in Fig. 1, solutions corresponding to tractions and body forces in the x- and z-directions, acting over annular and toroidal elements, shown in Fig. 4, are required. These solutions could be developed by integrating the solutions given by eqns (A1)–(A6) in the radial direction for the case of an annular element, and integration in both the r- and z-directions for a toroidal element. In performing integration in a radial direction, it is assumed that the asymmetric normal tractions acting on an annular element, and the asymmetric normal body force acting on a toroidal element, have linearly varying distributions in a radial direction. This enables convenient explicit integration in the radial direction. The expressions for displacement in the k-direction ($k = r, \theta, z$) at point $P_i(r_i, z_i)$ due to tractions or body forces in the l-direction ($l = x, z$) acting on element j with coordinates (r_j, z_j) are denoted by $f^{kl}(r_i, \theta, z_i; r_j, z_j)$. Explicit representation of f^{kl} for annular and toroidal elements are given by eqns (A18)–(A30) in the appendix.

ELASTIC CYLINDRICAL BAR EMBEDDED IN A HALF-SPACE

Figure 1 shows a cylindrical elastic bar of radius a and length h ($h/a \gg 1$) partially embedded in a surrounding elastic half-space. A cylindrical coordinate system (r, θ, z) is defined such that the z-axis coincides with the longitudinal centroidal axis of the cylinder and is normal to the stress-free surface of the half-space. The material properties of the bar, which is assumed to behave as a Bernoulli–Euler beam, are characterized by its Young's modulus E_b, and mass density ρ_b. The surrounding half-space is characterized by

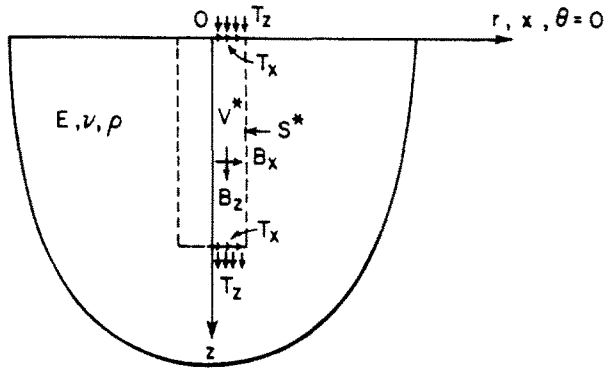

Fig. 5. Extended half-space subjected to body forces and end tractions.

its Young's modulus, Poisson's ratio and mass density denoted by E, ν, and ρ, respectively. It is assumed that the bar is continuously bonded to the surrounding half-space along the shaft of the bar ($r = a$, $0 \leqslant \theta \leqslant 2\pi$, $0 \leqslant z \leqslant h$) and along the base of the bar. The bar–half-space system is subjected either to a harmonic horizontal load $H_0 e^{i\omega t}$ acting in the x-direction or to a harmonic moment $M_0 e^{i\omega t}$ about the y-axis. These loadings are assumed to act at the top end of the bar at $z = 0$. Under these geometric and loading configurations, the system possesses symmetry about the x-axis ($\theta = 0$).

The method of analysis employed in this study is based on that proposed by Rajapakse and Shah[14] to solve the problem of longitudinal harmonic motion of a long cylindrical bar embedded in an elastic half-space. Initially, we consider the case of a short rigid cylindrical bar and apply the discretization procedure developed in Ref. [14]. Our objective at this stage is to verify the accuracy of the discretization procedure by comparing the solutions with those obtained by Apsel[12] for a short rigid cylinder under the action of a lateral load or a moment.

For this purpose, we consider the extended half-space–fictitious bar model originally proposed by Muki and Sternberg[2]. When the bar is rigid, it is unnecessary to consider a fictitious bar and consequently the assumption of the Bernoulli–Euler beam theory is no longer required. Consideration is given only to the extended half-space as shown in Fig. 5. It is assumed that volume V^* in the extended half-space (identical to that of the bar) is subjected to unknown body force distributions in the x- and z-directions (with variation in the θ-direction as shown in Figs 3(a) and (b)). In addition, the terminal cross-sections at $z = 0$ and h are subjected to unknown traction distributions in the x- and z-directions, simulating direct load transfers to the surrounding half-space. When the bar is long, it is reasonable to assume that the effect of body forces in the z-direction and concentrated load transfers in the z-direction at the terminal cross-sections can be neglected.

For the static problem involving a long cylindrical bar, the body force in the x-direction in V^* and traction in the x-direction at the terminal cross-sections could be assumed to have a uniform distribution. Under these assumptions, the model of Apirathvorakij and Karasudhi[1] is obtained. For elastodynamic problems, it was found in Ref. [14] that solutions based on a uniform body force and traction model are accurate only in the very low frequency range. In this study, as in Ref. [14], it is assumed that body forces and tractions are distributed nonuniformly within a cross-section of V^*. However, it should be mentioned here that the displacements in V^* due to a non-uniform body force and traction field generated by fundamental loadings shown in Fig. 2 would not correspond exactly to a rigid body mode of V^*, due to azimuthal dependence of the problem. In view of this displacement compatibility is proposed to impose along the x-axis ($\theta = 0$).

Thereafter, the volume V^* is discretized by toroidal elements, and the terminal cross-sections are discretized by annular elements shown in Fig. 4. A flexibility equation relating to the magnitude of the body forces acting on toroidal elements, and traction acting on annular elements could be established through the influence functions $\bar{f}^{kl}(r_i, \theta, z_i; r_j, z_j)$

and $\bar{f}^{kl}(r_i, \theta, z_i; r_j, z_j)$ given in the appendix, to ensure that the x–z plane in domain V^* moves as the rigid body. The appropriate rigid body displacements for a point in the x–z plane ($\theta = 0$) are

$$u = \Delta_h + (h - z)\phi_0 \tag{8a}$$

$$w = r\phi_0 \tag{8b}$$

where Δ_h is the displacement in the x-direction at $z = h$ and ϕ_0 is the rotation about the y-axis. The appropriate flexibility equation can be written as

$$\sum_{j=1}^{M_1} [\bar{f}^{rx}(r_i, 0, z_i; r_j, z_j)B_{xj} + \bar{f}^{rz}(r_i, 0, z_i; r_j, z_j)B_{zj}] + \sum_{j=1}^{M_2} [\bar{f}^{rx}(r_i, 0, z_i; r_j, z_j)T_{xj} + \bar{f}^{rz}(r_i, 0, z_i; r_j, z_j)T_{zj}] - \Delta_h - (h - z_i)\phi_0 = 0 \qquad (i = 1, \ldots, M_1 + M_2) \tag{9a}$$

$$\sum_{j=1}^{M_1} [\bar{f}^{zx}(r_i, 0, z_i; r_j, z_j)B_{xj} + \bar{f}^{zz}(r_i, 0, z_i; r_j, z_j)B_{zj}] + \sum_{j=1}^{M_2} [\bar{f}^{zx}(r_i, 0, z_i; r_j, z_j)T_{xj} + \bar{f}^{zz}(r_i, 0, z_i; r_j, z_j)T_{zj}] - r_i\phi_0 = 0 \qquad (i = 1, \ldots, M_1 + M_2) \tag{9b}$$

$$\sum_{j=1}^{M_1} 2\pi r_j \Delta z_j \Delta r_j B_{xj} + \sum_{j=1}^{M_2} 2\pi r_j T_{xj} \Delta r_j + \pi a^2 h\omega^2(\rho - \rho_b)(\Delta_h + h\phi_0/2) = H_0 \tag{9c}$$

$$\sum_{j=1}^{M_1} \left\{2\pi r_j(h - z_j)\Delta z_j \Delta r_j B_{xj} + \frac{\pi}{4}[(r_j + \Delta r_j/2)^4 - (r_j - \Delta r_j/2)^4]\Delta z_j B_{zj}\right\} + \sum_{j=1}^{M_2} \left\{2\pi r_j(h - z_j)\Delta r_j T_{xj} + \frac{\pi}{4}[(r_j + \Delta r_j/2)^4 - (r_j - \Delta r_j/2)^4]T_{zj}\right\} \pi a^2 h\omega^2(\rho - \rho_b)[h^2\phi_0/3 + \Delta_h h/2] + \pi h a^4 \omega^2(\rho - \rho_b)\phi_0/4 = M_0. \tag{9d}$$

In eqns (9a)–(9d), B_{xj} and B_{zj} denote the intensity of body forces in the x- and z-directions acting on the jth toroidal element; T_{xj} and T_{zj} denote the intensity of tractions in the x- and z-directions acting on the jth annular element modelling terminal cross-sections; M_1 and M_2 are the total number of toroidal and annular elements employed to model the volume V^* and terminal cross-sections, respectively. The solution of eqns (9a)–(9d) with either $H_0 = 1$ and $M_0 = 0$ or $H_0 = 0$ and $M_0 = 1$ would yield the numerical values of B_{xj}, B_{zj} ($j = 1, \ldots, M_1$), T_{xj}, T_{zj} ($j = 1, \ldots, M_2$), Δ_0 and ϕ_0. Thereafter, horizontal impedance k_H ($H_0/\mu a\Delta_h$), rotational impedance $k_M(M_0/\mu a^3\phi_0)$, and coupled impedance K_{MH} or k_{HM} ($H_0/\mu a^2\phi_0$ or $M_0/\mu a^2\Delta_h$) could be determined.

Figure 6 shows the comparison of real (Re) and imaginary (Im) parts of rotational impedance of a massless rigid cylinder ($h/a = 2.0$) obtained from the present study with those obtained by Apsel[12]. In Fig. 6, the non-dimensional frequency a_0 is defined as $a_0 = ak_s$. The results obtained from the present scheme for k_H agree well with those of Apsel[12] for $0 < a_0 < 1.0$. This confirms the accuracy of assumptions employed on body force fields, the computation of influence functions given in the appendix and the discretization technique within the low frequency range of interest.

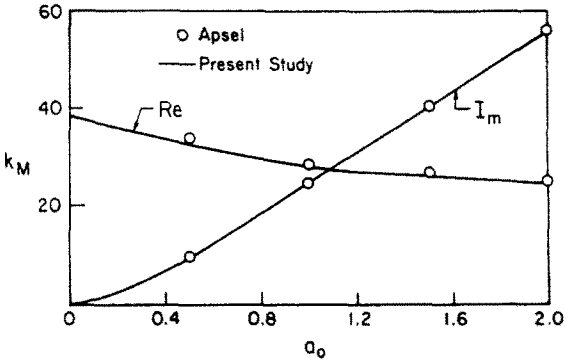

Fig. 6. Comparison of rotational impedance of a rigid cylinder embedded in a half-space ($h/a = 2.0$, $\nu = 0.25$, $M_1 = 40$, $M_2 = 10$).

In the case of an elastic bar in addition to the extended half-space, a fictitious bar with Young's modulus $E^*(E^* = E_b - E)$ and density $\rho^*(\rho^* = \rho_b - \rho)$ has to be considered. Unlike in the case of a rigid bar, the variation of displacements of the region V^* of the extended half-space (in turn that of the fictitious bar) is not known beforehand. By restricting ourselves to the case of a long elastic bar excited in the low frequency range, it is reasonable to assume that the bar is governed by the Euler–Bernoulli beam theory and the effects of body force in the z-direction in V^* and tractions in the z-direction acting on terminal cross-sections are negligible. Based on the above assumptions, the displacement of the bar in the x-direction, u, can be approximated in the following form

$$u(z,t) = \sum_{n=1}^{N} a_n[\alpha_n - e^{-nz/h}] \tag{10a}$$

$$\dot{u}(z,t) = \sum_{n=1}^{N} \dot{a}_n[\alpha_n - e^{-nz/h}] \tag{10b}$$

where $a_1,\ldots,a_N$ could be considered as generalized coordinates which remain unknown at this stage, and the superscript dot denotes differentiation with respect to time. The quantities $\alpha_1,\ldots,\alpha_N$ are necessary to satisfy the appropriate equilibrium conditions (i.e. total moment acting on the system should be zero under the application of a horizontal force or vice versa). The body force field in the x-direction in V^* and the traction in the x-direction in terminal cross-sections which produce a displacement field identical to that given by eqns (10a) and (10b) in V^* along the x-axis ($\theta = 0$) could be determined by establishing a flexibility equation in the following form for each term of eqn (10a) with $a_n = 1$

$$\sum_{j=1}^{M_1} f^{rx}(r_i,0,z_i;r_j,z_j)B_{xj}^n + \sum_{j=1}^{M_2} f^{rx}(r_i,0,z_i;r_j,z_j)T_{xj}^n - \alpha_n = -e^{-nz_i/h} \qquad (i = 1,\ldots,M_1+M_2) \tag{11a}$$

$$\sum_{j=1}^{M_1} 2\pi r_j \Delta r_j z_j B_{xj}^n + \sum_{j=1}^{M_2} 2\pi r_j \Delta r_j T_{xj}^n = 0 \tag{11b}$$

$$\sum_{j=1}^{M_1} 2\pi r_j \Delta r_j \Delta z_j z_j B_{xj}^n + \sum_{j=1}^{M_2} 2\pi r_j \Delta r_j z_j T_{xj}^n = 0. \tag{11c}$$

If the bar–half-space system is subjected to a horizontal force, then eqns (11a) and (11c) are solved for T_{xj}^n, T_{xj}^n, and α_n. If the system is subjected to a moment, then eqns (11a)

and (11b) are solved to obtain T^n_{xj}, T^n_{xj}, α_n. The body force B_{xj} and traction T_{xj} acting on the jth toroidal and annular required to produce the displacement field given by eqn (10a) can be expressed as

$$B_{xj} = \sum_{n=1}^{N} a_n B^n_{xj} \tag{12a}$$

$$T_{xj} = \sum_{n=1}^{N} a_n T^n_{xj}. \tag{12b}$$

At this stage, consider the strain energy U_b and kinetic energy T_b of the fictitious bar. It is found that in view of eqns (10a) and (10b)

$$U_b = \sum_{n=1}^{N}\sum_{m=1}^{N} D_{mn} a_n a_m \tag{13}$$

$$T_b = \sum_{n=1}^{N}\sum_{m=1}^{N} C_{mn} \dot{a}_n \dot{a}_m \tag{14}$$

where

$$D_{mn} = \frac{E^* \pi a^4 n^2 m^2}{8h^3(n+m)}(1 - e^{-(n+m)}) \tag{15a}$$

$$C_{mn} = \frac{\pi a^2 \rho^* h}{2}\left[\alpha_n \alpha_m + \frac{\alpha_n e^{-m}}{m} + \frac{\alpha_m e^{-n}}{n} - \frac{h e^{-(m+n)}}{(m+n)}\right] \tag{15b}$$

Note that in eqn (14), the contribution to the kinetic energy due to the velocity component in the z-direction is neglected. The effect of this component is discussed in a subsequent section.

Introducing standard indicial notation, the Lagrangian[16] for the extended half-space can be written as[14]

$$L_h = \frac{1}{2}\frac{\partial}{\partial t}\int_V \rho u_i \dot{u}_i \, dv - \frac{1}{2}\int_{S_1} u_i T_i \, ds - \frac{1}{2}\int_{S_2} u_i T_i \, ds - \frac{1}{2}\int_{V^*} u_i B_i \, dv. \tag{16}$$

In eqn (16), V denotes the volume of the extended half-space, S_1 and S_2 are the areas of terminal cross-sections at $z = 0$ and h, respectively. Further, note that the displacement, velocity, acceleration, tractions and body forces in V can be expressed in terms of the generalized coordinates.

The application of Lagrange's equation of motion[16, 17] to the total system, composed of extended half-space and fictitious bar, together with eqns (10)–(16) results in the following algebraic equations of motion for $H_0 e^{i\omega t}$s, when the bar–half-space system is subjected to horizontal force $H_0 e^{i\omega t}$

$$\sum_{n=1}^{N} a_n[-2\omega^2 C_{ni} + 2D_{ni} + \pi \sum_{j=1}^{M_2} r_j(T^i_{zj}E_{nj} + T^n_{zj}E_{ij})\Delta r_j + \pi \sum_{j=1}^{M_1} r_j(B^i_{zj}E_{nj} + B^n_{zj}E_{ij})\Delta z_j \Delta r_j] = H_0[\alpha_i - 1] \quad (i = 1, \ldots, N) \tag{17}$$

where $E_{nj} = [\alpha_n - e^{-n z_j/h}]$.

When the bar–half-space system is subjected to a moment $M_0 e^{i\omega t}$, the appropriate

Table 1. Dependence of k_H and k_{MH} on the number of toroidal elements (M_1) and the number of annular elements (M_2): $h/a = 10$, $\bar{\rho} = 1.0$, $\nu = 0.25$, $N = 8$, $a_0 = 1.0$

(M_1, M_2)	k_H		k_{MH}	
	$\bar{E} = 10$	$\bar{E} = 250$	$\bar{E} = 10$	$\bar{E} = 250$
(20, 4)	(4.97, 5.46)	(7.35, 15.31)	(11.36, 4.78)	(52.79, 42.74)
(40, 8)	(5.22, 6.04)	(7.50, 15.43)	(12.71, 5.61)	(53.56, 43.04)
(60, 6)	(5.27, 6.10)	(7.58, 15.86)	(12.89, 5.63)	(54.24, 43.70)
(80, 8)	(5.30, 6.15)	(7.60, 15.91)	(12.94, 5.65)	(54.41, 43.96)

equations of motion are given by eqns (17) with the exception that the term $H_0(\alpha_i - 1)$ on the right-hand side is replaced by $M_0 i/h$. Solution of eqns (17) yields the numerical values a_i $(i = 1, \ldots, N)$, and the horizontal displacement Δ_0 and rotation ϕ_0 at the top end of the bar $(z = 0)$ are given by

$$\Delta_0 = \sum_{n=1}^{N} a_n[\alpha_n - 1] \tag{18}$$

$$\phi_0 = \sum_{n=1}^{N} a_n \frac{n}{h}. \tag{19}$$

DISCUSSION AND CONCLUSIONS

The first step of the parametric study is to determine the convergence of the numerical solution with respect to the number of toroidal elements (M_1) and annular elements (M_2) used in the discretization of V^* and the number of terms, N, used in the displacement approximation given by eqn (10a). The non-dimensionalized impedances k_H, k_M, k_{MH}, and k_{HM} of the bar–half-space system shown in Fig. 1 are defined as

$$k_H = H_0/\mu a \Delta_0, \qquad k_M = M_0/\mu a^3 \phi_0$$
$$k_{MH} = H_0/\mu a^2 \phi_{0H}, \qquad k_{HM} = M_0/\mu a^2 \Delta_{0M}$$

where Δ_0 and ϕ_{0H} are the displacement in the x-direction and rotation about the y-axis at the top end of the bar under the application of horizontal force H_0. The rotation about the y-axis and displacement in the x-direction at the top end of the bar under moment M_0 is denoted by ϕ_0 and Δ_{0M}, respectively.

Table 1 presents the dependence of impedances k_H and k_{MH} of an elastic bar–half-space system [$h/a = 10$, $\nu = 0.25$, $\bar{\rho} = 1.0$ ($\bar{\rho} = \rho_b/\rho$), $N = 8$, $a_0 = 1.0$] on a number of toroidal elements (M_1) and annular elements (M_2) employed to discretize V^*. Numerical solutions are presented in Table 1 for $\bar{E} = 10$ and 250, where $\bar{E} = E_b/E$. The dependence of impedances k_H, k_M, k_{MH} on the number of terms (N) used in the displacement approximation given by eqn (10a) is presented in Table 2. It is noted that numerical results obtained for coupled components k_{MH} and k_{HM} satisfy the reciprocal condition under lateral and moment loading.

In addition to the above convergence study, solutions were obtained for k_H, k_M, k_{MH} and k_{HM} by approximating the displacement u of the bar as $u = \sum_{n=1}^{N} a_n[\alpha_n - (z/h)^n]$. The impedances obtained by solving the appropriate equations of motion were found to be almost identical to those obtained on the basis of eqn (10a) as seen from Table 2. Due to

Table 2. Convergence of the horizontal, moment and coupled impedance of an elastic bar for different function bases and number of terms (N): $h/a = 10$, $\bar{E} = 10.0$, $\bar{\rho} = 1.0$, $\nu = 0.25$, $M_1 = 80$, $M_2 = 8$

N	a_o = 1.0					
	K_H		K_M		K_{HM}, K_{MH}	
	Expon.	Polyno.	Expon.	Polyno.	Expon.	Polyno.
2	(3.70, 6.45)	(2.96, 9.13)	(11.93, 13.34)	(23.28, 41.94)	(8.20, 10.01)	(10.46, 22.16)
4	(4.90, 6.17)	(5.26, 6.79)	(11.38, 1.92)	(11.29, 2.11)	(12.56, 5.98)	(12.37, 4.93)
6	(3.78, 5.68)	(5.27, 6.13)	(11.76, 2.62)	(11.44, 1.80)	(11.30, 7.73)	(12.92, 5.69)
8	(5.30, 6.15)	(5.25, 6.16)	(11.44, 1.79)	(11.44, 1.82)	(12.94, 5.65)	(12.92, 5.74)
10	(5.30, 6.15)	(5.25, 6.15)	(11.44, 1.79)	(11.44, 1.82)	(12.94, 5.65)	(12.91, 5.74)
12	(5.30, 6.15)	(5.25, 6.15)	(11.44, 1.79)	(11.44, 1.82)	(12.94, 5.65)	(12.91, 5.74)

Table 3. Comparison of impedances obtained using different compatibility conditions: $h/a = 10$, $\nu = 0.25$, $N = 8$, $a_0 = 1.0$, $M_1 = 60$, $M_2 = 6$

(M_1, M_2)	k_H		k_{MH}	
	Compatibility along θ=0 (x-axis)	Circum. Avg. Compatibility	Compatibility along θ=0 (x-axis)	Circum. Avg. Compatibility
10	(5.27, 6.10)	(5.33, 6.17)	(12.89, 5.63)	(12.81, 5.71)
250	(7.58, 15.86)	(7.93, 16.20)	(54.24, 43.70)	(55.29, 43.87)
1000	(5.15, 20.31)	(5.45, 20.91)	(63.66, 106.17)	(66.10, 108.10)
5000	(3.51, 21.39)	(3.73, 22.06)	(39.79, 138.9)	(41.49, 142.60)

the azimuthal dependence of the problem, the displacement in the x-direction in V^* due to body force B_x would be θ dependent. Thus, a variety of compatibility conditions could be considered between the domain V^* of the extended half-space and the fictitious bar. In this study, displacement compatibility is imposed along the x-axis ($\theta = 0$) of V^* and the fictitious bar. In addition to this, we have investigated a solution which is based on compatibility between the circumferential average displacement of V^* in the x-direction and the fictitious bar. Solutions obtained from these two compatibility conditions are compared in Table 3. In deriving the kinetic energy of the fictitious bar as given by eqn (14), the velocity component in the z-direction was neglected. In a separate study, the influence of this velocity component was taken into account, and the numerical solutions were found to differ by less than 5% from those based on eqn (14).

Figures 7–9 illustrate the influence of the flexibility ratio $\bar{E}$ and the non-dimensionalized frequency parameter a_0 ($0 \leqslant a_0 \leqslant 1.0$) on the horizontal, moment and coupled impedances of an elastic bar–half-space system for $h/a = 10$ and 20 ($\bar{\rho} = 1.0, \nu = 0.25$). It appears from Fig. 7 that the real part of the horizontal impedance shows a gradual decrease with increasing frequency. As the bar becomes rigid (as $\bar{E}$ increases) the decrease in the real part of the horizontal impedance is more pronounced, reflecting the dominance of the inertia component. The variation in the imaginary part of the horizontal impedance is almost linear with increasing a_0 for both flexible and stiff bars. The rotational impedances plotted in Fig. 8 are normalized with respect to the static value obtained by Karasudhi *et al.*[3]. The reason for this normalization is due to the fact that non-normalized rotational

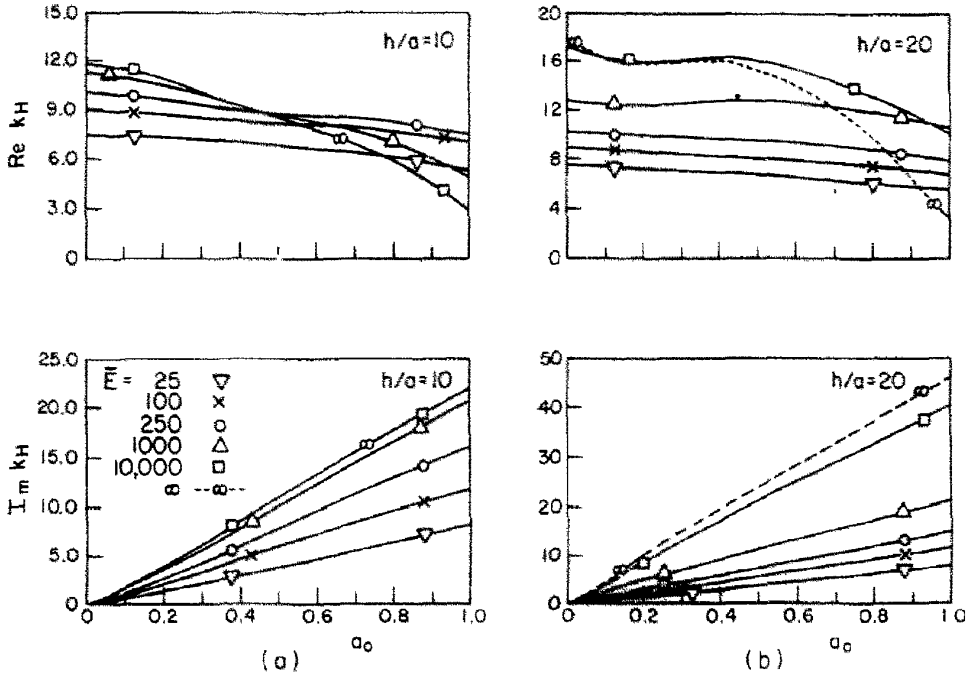

Fig. 7. Variation of horizontal impedance (k_H) of a cylindrical elastic bar for various $\bar{E}$ ($\nu = 0.25$, $\bar{\rho} = 1.0$, $M_1 = 40$, $M_2 = 8$ for $h/a = 10$, $M_1 = 60$, $M_2 = 6$ for $h/a = 20$).

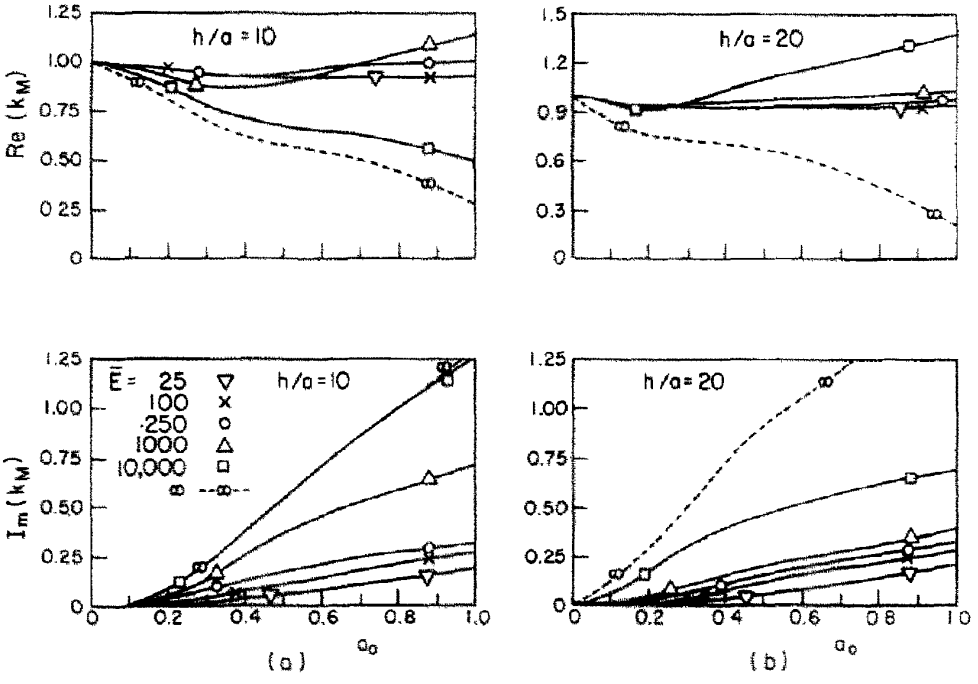

Fig. 8. Variation of rotational impedance (k_M) of a cylindrical elastic bar for various $\bar{E}$ ($\nu = 0.25$, $\bar{\rho} = 1.0$, $M_1 = 40$, $M_2 = 8$ for $h/a = 10$, $M_1 = 60$, $M_2 = 6$ for $h/a = 20$).

impedance for a bar with $\bar{E} = 25$ is very small compared to that for $\bar{E} = 10{,}000$, making it difficult to represent rotational impedances for a wide range of $\bar{E}$ values in one figure. In general, the variation in the real part of k_M is similar to that observed for the axial impedance in Ref. [14]. When the bar is quite flexible, $\mathrm{Re}(k_M)$ shows little dependence on a_0 and as $\bar{E}$ increases, $\mathrm{Re}(k_M)$ increases with frequency. As the bar becomes stiffer

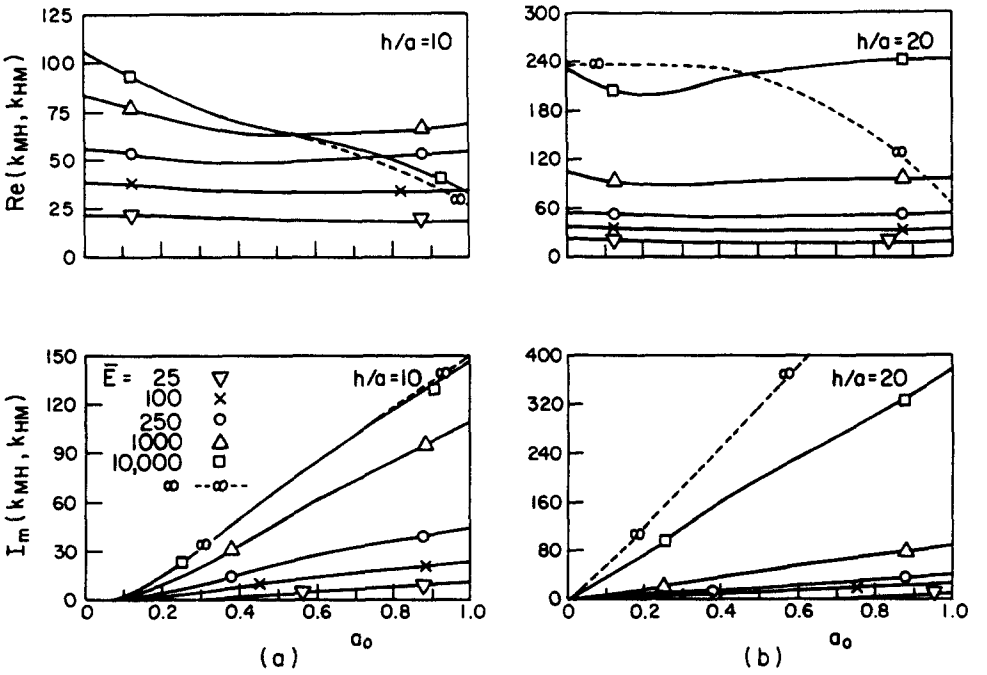

Fig. 9. Variation of coupled impedance (k_{MH}, k_{HM}) of a cylindrical elastic bar for various $\bar{E}$ ($\nu = 0.25$, $\bar{\rho} = 1.0$, $M_1 = 40$, $M_2 = 8$ for $h/a = 10$, $M_1 = 60$, $M_2 = 6$ for $h/a = 20$).

($\bar{E} \to \infty$), $\mathrm{Re}(k_M)$ shows a typical sharp drop with increasing a_0 characterizing the influence of inertia. As for the imaginary part of k_M, the variation with a_0 is linear except in the very low frequency near the static solution. The coupled impedances k_{MH} and k_{HM} plotted in Fig. 9 follow behaviour similar to the horizontal impedance.

From the results presented in Figs 7–9, it is evident that the relative flexibility parameter of the bar–half-space system is governed by $\bar{E}$, the h/a ratio, and the type of loading (i.e. lateral or moment). This also suggests that in most practical situations, long piles behave as flexible piles rather than as rigid piles under transverse loading.

Figure 10 illustrates the variation of horizontal and rocking impedances of an elastic bar ($h/a = 10.0$, $\bar{E} = 100$, $\nu = 0.25$) in the frequency range $a_0 = 0$–1.0 for different mass density ratios ($\bar{\rho}$). Horizontal impedance shows higher dependence on $\bar{\rho}$ than the moment impedance. The dependence of coupled impedance on $\bar{\rho}$ is found to be similar to that of moment impedance. It should be mentioned here that for highly flexible bars (e.g. $h/a = 10$, and $\bar{E} < 50$), the dependence of impedances on $\bar{\rho}$ may be negligible for $a_0 < 1.0$. On the other hand, if the relative flexibility is such that the behaviour of the bar is closer to that of a rigid bar, impedances show considerable dependence on a_0 for $a_0 > 0.25$.

In conclusion, an accurate solution scheme based on Lagrange's equation of motion is presented to study the lateral harmonic vibrations of a long elastic bar embedded in a homogeneous half-space and subjected to a harmonic lateral load or a moment. In the authors' opinion, the analysis presented in this study together with those in Ref. [14] presents the most accurate estimation at present for the impedance matrix of a single pile under the three basic modes of loading over a wide range of frequencies.

Acknowledgement—The work presented here was supported by grant A-7988 from the Natural Science and Engineering Research Council of Canada.

REFERENCES

1. V. Apirathvorakij and P. Karasudhi, Quasistatic bending of a cylindrical elastic bar partially embedded in a saturated elastic half space. *Int. J. Solids Structures* **16**, 625 (1980).
2. R. Muki and E. Sternberg, Elastostatic load transfer to a half space from a partially embedded axially loaded rod. *Int. J. Solids Structures* **6**, 69 (1970).

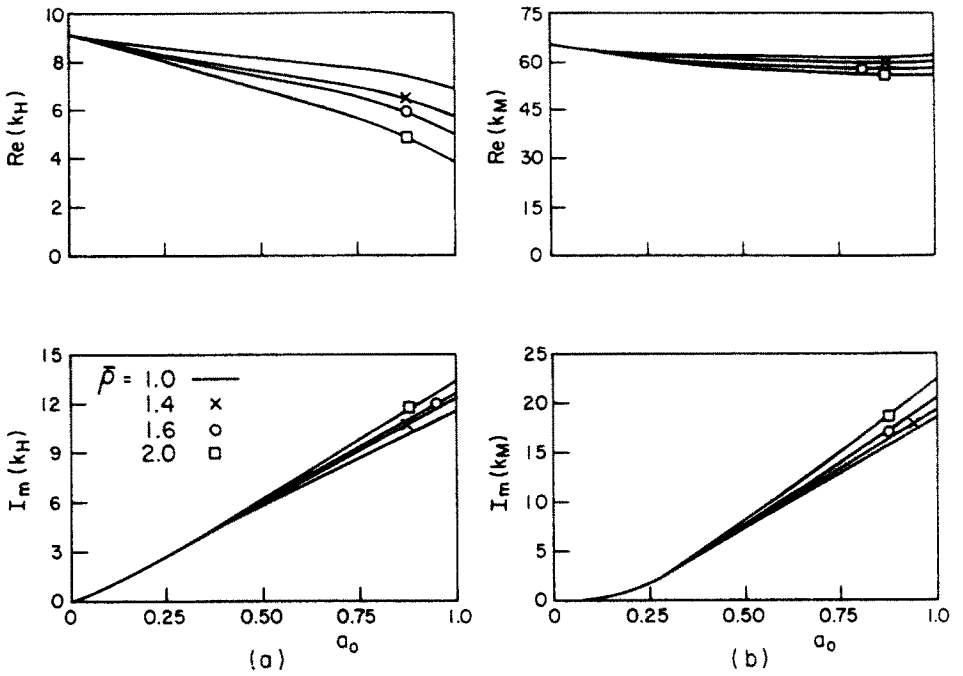

Fig. 10. Variation of horizontal and rotational impedances (k_H and k_M) of a cylindrical elastic bar for different density ratios ($h/a = 10.0$, $\bar{E} = 100.0$, $\nu = 0.25$, $M_1 = 40$, $M_2 = 8$).

3. P. Karasudhi, R. K. N. D. Rajapakse and K. K. Liyanage, A reconsideration of elastostatic load transfer problems involving a half space. *Trans. CSME* **8**, 219 (1984).
4. W. R. Spillers and R. D. Stoll, Lateral response of piles. *J. Soil Mech. Found. ASCE* **90**, 1 (1964).
5. R. D. Mindlin, Nuclei of strain in the semi-infinite solid. *J. Appl. Phys.* **21**, 926 (1950).
6. H. G. Poulos, Behaviour of laterally loaded piles: 1. Single piles. *J. Soil Mech. Found. ASCE* **97**, 711 (1971).
7. R. Butterfield and P. K. Bannerjee, The elastic analysis of compressible piles and pile groups. *Geotechnique* **21**, 43 (1971).
8. A. P. S. Selvadurai and R. K. N. D. Rajapakse, On the load transfer from a rigid cylindrical inclusion into an elastic half space. *Int. J. Solids Structures* **21**, 1213 (1985).
9. T. Nogami and M. Novak, Resistance of soil to a horizontally vibrating pile. *Earthquake Engng Struct. Dyn.* **5**, 249 (1977).
10. M. Novak and T. Nogami, Soil pile interaction in horizontal vibration. *Earthquake Engng Struct. Dyn.* **5**, 263 (1977).
11. M. T. Nielsen, Resistance of a soil layer to horizontal vibration of a pile. *Earthquake Engng Struct. Dyn.* **10**, 497 (1982).
12. R. J. Apsel, Dynamic Green's function for layered media and application to boundary value problems. Ph.D. Dissertation, University of California, San Diego, California (1979).
13. R. Sen, T. G. Davies and P. K. Bannerjee, Dynamic analysis of piles and pile groups embedded in homogeneous soils. *Earthquake Engng Struct. Dyn.* **13**, 53 (1985).
14. R. K. N. D. Rajapakse and A. H. Shah, On the longitudinal harmonic motion of a long cylindrical elastic bar embedded in an elastic half space. *Int. J. Solids Structures* **23**, 267–285 (1987).
15. I. N. Sneddon, *Fourier Transforms*. McGraw-Hill, New York (1951).
16. K. Washishu, *Variational Methods in Elasticity and Plasticity*, 3rd Edn. Pergamon, Oxford (1982).
17. S. S. Rao, *The Finite Element Method in Engineering*, 1st Edn, Pergamon, Oxford (1982).

APPENDIX

The following are expressions for displacements corresponding to concentrated ring forces shown in Fig. 3

Concentrated ring force in the x-direction (Fig. 3(a))

$$u(r,\theta,z;s,z') = \cos\theta \int_0^\infty \beta R_1(\xi) F_1(\xi,z,z') s\xi J_0(\xi s) G_1(\xi r)\,d\xi + \int_0^\infty R_2(\xi) F_2(\xi,z,z') s\xi J_0(\xi s) G_2(\xi r)\,d\xi \quad \text{(A1)}$$

$$v(r,\theta,z;s,z') = \sin\theta\int_0^\infty \beta R_1(\xi)F_1(\xi,z,z')s\xi J_0(\xi s)G_2(\xi r)\,d\xi + \int_0^\infty R_2(\xi)F_2(\xi,z,z')s\xi J_0(\xi s)G_1(\xi r)\,d\xi \tag{A2}$$

$$w(r,\theta,z;s,z') = \cos\theta\int_0^\infty 2\alpha\beta R_1(\xi)F_3(\xi,z,z')s\xi^2 J_0(\xi s)J_1(\xi r)\,d\xi. \tag{A3}$$

Concentrated ring force in the z-direction with azimuthal dependence (Fig. 3(b))

$$u(r,\theta,z;s,z') = \cos\theta\int_0^\infty \alpha\beta R_1(\xi)F_4(\xi,z,z')s\xi^2 J_1(\xi s)G_1(\xi r)\,d\xi \tag{A4}$$

$$v(r,\theta,z;s,z') = \sin\theta\int_0^\infty \alpha\beta R_1(\xi)F_4(\xi,z,z')s\xi^2 J_1(\xi s)G_2(\xi r)\,d\xi \tag{A5}$$

$$w(r,\theta,z;s,z') = \cos\theta\int_0^\infty 2\alpha R_1(\xi)F_5(\xi,z,z')s\xi J_1(\xi s)J_1(\xi r)\,d\xi. \tag{A6}$$

The functions $F_1(\xi, z, z')$, $F_2(\xi, z, z'), \ldots, F_5(\xi, z, z')$ and $R_1(\xi)$ appearing in eqns (A1)–(A6) are defined as

$$F_1(\xi,z,z') = 4\alpha\beta\xi^2(2\xi^2 - k_s^2)(Q_1 + Q_2) + R(\xi)(\xi^2 Q_3 - \alpha\beta Q_4) - \bar{R}(\xi)(\xi^2 Q_5 + \alpha\beta Q_6) \tag{A7}$$

$$F_2(\xi,z,z') = Q_6 + Q_4 \tag{A8}$$

$$F_3(\xi,z,z') = 4(2\xi^2 - k_s^2)(\alpha\beta Q_1 + \xi^2 Q_2) + \eta R(\xi)(Q_3 - Q_4) - \bar{R}(\xi)(Q_5 + Q_6) \tag{A9}$$

$$F_4(\xi,z,z') = -[4(2\xi^2 - k_s^2)(\xi^2 Q_1 + \alpha\beta Q_2) + \eta R(\xi)(Q_3 - Q_4) - \bar{R}(\xi)(Q_5 + Q_6)] \tag{A10}$$

$$F_5(\xi,z,z') = -[4\alpha\beta\xi^2(2\xi^2 - k_s^2)(Q_1 + Q_2) + R(\xi)(\xi^2 Q_4 - \alpha\beta Q_3) - \bar{R}(\xi)(\xi^2 Q_6 + \alpha\beta Q_5)] \tag{A11}$$

$$R_1(\xi) = -\frac{1}{4\mu\alpha\beta k_s^2 R(\xi)} \tag{A12}$$

$$R_2(\xi) = \frac{1}{4\mu\beta} \tag{A13}$$

$$R(\xi) = (2\xi^2 - k_s^2)^2 - 4\alpha\beta\xi^2 \tag{A14a}$$

$$\bar{R}(\xi) = (2\xi^2 - k_s^2)^2 + 4\alpha\beta\xi^2 \tag{A14b}$$

$$G_1(\xi r) = J_2(\xi r) - J_0(\xi r);\ G_2(\xi r) = J_2(\xi r) + J_0(\xi r) \tag{A15}$$

$$\eta = -1 \quad \text{if } z < z'$$
$$= \ \ 1 \quad \text{if } z > z' \tag{A16}$$

$$Q_1 = e^{-\alpha z - \beta z'},\quad Q_2 = e^{-\alpha z' - \beta z},\quad Q_3 = e^{-\alpha|z - z'|}$$
$$Q_4 = e^{-\beta|z - z'|},\quad Q_5 = e^{-\alpha(z + z')},\quad Q_6 = e^{-\beta(z + z')}. \tag{A17}$$

The following are the expressions for displacements corresponding to distributed tractions acting on an annular element (Fig. 4).

Uniform traction in the x-direction

$$f^{rx}(r_i,\theta,z_i;r_j,z_j) = \cos\theta\left[\int_0^\infty \beta R_1(\xi)F_1(\xi,z_i,z_j)sJ_1(\xi s)G_1(\xi r_i)\,d\xi + \int_0^\infty R_2(\xi)F_2(\xi,z_i,z_j)sJ_1(\xi s)G_2(\xi r_i)\,d\xi\right]_{s=z_{j1}}^{s=z_{j2}} \tag{A18}$$

$$f^{\theta x}(r_i,\theta,z_i;r_j,z_j) = \sin\theta\left[\int_0^\infty \beta R_1(\xi)F_1(\xi,z_i,z_j)sJ_1(\xi s)G_2(\xi r_i)\,d\xi + \int_0^\infty R_2(\xi)F_2(\xi,z_i,z_j)sJ_1(\xi s)G_2(\xi r_i)\,d\xi\right]_{s=z_{j1}}^{s=z_{j2}} \tag{A19}$$

$$\bar{f}^{zz}(r_i,\theta,z_i;r_j,z_j)=\cos\theta\left[\int_0^{\infty}2\alpha\beta R_1(\xi)F_3(\xi,z_i,z_j)s\xi J_1(\xi s)J_1(\xi r_i)\,d\xi\right]_{s=s_{j1}}^{s=s_{j2}} \tag{A20}$$

Traction in the z-direction (Fig. 3(b)) with a linear variation in the r-direction

$$\bar{f}^{rz}(r_i,\theta,z_i;r_j,z_j)=\cos\theta\left[\int_0^{\infty}\alpha\beta R_1(\xi)F_4(\xi,z_i,z_j)s^2\xi J_2(\xi s)G_1(\xi r_i)\,d\xi\right]_{s=s_{j1}}^{s=s_{j2}} \tag{A21}$$

$$\bar{f}^{\theta z}(r_i,\theta,z_i;r_j,z_j)=\sin\theta\left[\int_0^{\infty}\alpha\beta R_1(\xi)F_4(\xi,z_i,z_j)s^2\xi J_2(\xi s)G_2(\xi r_i)\,d\xi\right]_{s=s_{j1}}^{s=s_{j2}} \tag{A22}$$

$$\bar{f}^{zz}(r_i,\theta,z_i;r_j,z_j)=\cos\theta\left[\int_0^{\infty}2\alpha\beta R_1(\xi)F_5(\xi,z_i,z_j)s^2J_2(\xi s)J_1(\xi r_i)\,d\xi\right]_{s=s_{j1}}^{s=s_{j2}} \tag{A23}$$

where

$$\begin{aligned}s_{j2}&=r_j+\Delta r_j/2\\ s_{j1}&=r_j-\Delta r_j/2.\end{aligned} \tag{A24}$$

The following are the expressions for displacements corresponding to body forces acting on a toroidal element (Fig. 4).

Body force in the x-direction with uniform distribution within the element

$$\begin{aligned}f^{rx}(r_i,\theta,z_i;r_j,z_j)=\cos\theta\Bigg[\int_0^{\infty}\{&\beta R_1(\xi)F_6(\xi,z_i,z')G_3(\xi s)G_1(\xi r_i)\\&+R_2(\xi)F_7(\xi,z_i,z')G_3(\xi s)G_2(\xi r_i)\}\,d\xi\Bigg]_{z'=z_{j1}}^{z'=z_{j2}}\end{aligned} \tag{A25}$$

$$\begin{aligned}f^{\theta x}(r_i,\theta,z_i;r_j,z_j)=\sin\theta\Bigg[\int_0^{\infty}\{&\beta R_1(\xi)F_6(\xi,z_i,z')G_3(\xi s)G_2(\xi r_i)\\&+R_2(\xi)F_7(\xi,z_i,z')G_3(\xi s)G_1(\xi r_i)\}\,d\xi\Bigg]_{z'=z_{j1}}^{z'=z_{j2}}\end{aligned} \tag{A26}$$

$$f^{zx}(r_i,\theta,z_i;r_j,z_j)=\cos\theta\left[\int_0^{\infty}2\alpha\beta R_1(\xi)F_8(\xi,z_i,z')\xi G_3(\xi s)J_1(\xi r_i)\,d\xi\right]_{z=z_{j1}}^{z'=z_{j2}} \tag{A27}$$

where $G_3(\xi s)=s_{j2}J_1(\xi s_{j2})-s_{j1}J_1(\xi s_{j1})$.

Body force in the z-direction with uniform distribution in the z-direction and linearly varying distribution in the r-direction

$$f^{rz}(r_i,\theta,z_i;r_j,z_j)=\cos\theta\left[\int_0^{\infty}\alpha\beta R_1(\xi)F_9(\xi,z_i,z')\xi G_4(\xi s)G_1(\xi r_i)\,d\xi\right]_{z'=z_{j1}}^{z'=z_{j2}} \tag{A28}$$

$$f^{\theta z}(r_i,\theta,z_i;r_j,z_j)=\sin\theta\left[\int_0^{\infty}\alpha\beta R_1(\xi)F_9(\xi,z_i,z')\xi G_4(\xi s)G_2(\xi r_i)\,d\xi\right]_{z'=z_{j1}}^{z'=z_{j2}} \tag{A29}$$

$$f^{zz}(r_i,\theta,z_i;r_j,z_j)=\cos\theta\left[\int_0^{\infty}2\alpha R_1(\xi)F_{10}(\xi,z_i,z')G_4(\xi s)J_1(\xi r_i)\,d\xi\right]_{z'=z_{j1}}^{z'=z_{j2}} \tag{A30}$$

where

$$\begin{aligned}G_4(\xi s)&=s_{j2}^2J_2(\xi s_{j2})-s_{j1}^2J_2(\xi s_{j2})\\ z_{j1}&=z_j-\Delta z_j/2\\ z_{j2}&=z_j+\Delta z_j/2\end{aligned} \tag{A31}$$

and

$$\begin{aligned}F_6(\xi,z,z')=4\alpha\beta\xi^2(2\xi^2-k_s^2)(-Q_1/\beta-Q_2/\alpha)+\eta R(\xi)(\xi^2Q_3/\alpha-\alpha Q_4)\\+\bar{R}(\xi)(\xi^2Q_5/\alpha+\alpha Q_6)\end{aligned} \tag{A32}$$

$$F_7(\xi,z,z')=-(Q_6/\beta-\eta Q_4/\beta) \tag{A33}$$

$$F_8(\xi,z,z')=-4(2\xi^2-k_s^2)(\alpha Q_1+\xi^2Q_2/\alpha)+R(\xi)(Q_3/\alpha-Q_4/\beta)+\bar{R}(\xi)(Q_5/\alpha+Q_6/\beta) \tag{A34}$$

$$F_9(\xi, z, z') = -[-4(2\xi^2 - k_2^2)(\xi^2 Q_1/\beta + \beta Q_2) + R(\xi)(Q_3/\alpha - Q_4/\beta) + \bar{R}(\xi)(Q_5/\alpha + Q_6/\beta)] \quad \text{(A35)}$$

$$F_{10}(\xi, z, z') = -[-4\alpha\beta\xi^2(2\xi^2 - k_2^2)(Q_1/\beta + Q_2/\alpha) + \eta R(\xi)(\xi^2 Q_4/\beta - \beta Q_3) + \bar{R}(\xi)(\xi^2 Q_6/\beta + \beta Q_5)]. \quad \text{(A36)}$$

The functions appearing in eqns (A18)–(A30) are evaluated by numerical integration along a contour in the first quadrant of the complex plane[14].